Chopper for the Beam EDM experiment

Anastasio Fratangelo

July 16, 2020

Contents

Chapter 1

Introduction

In this document, the realization of the chopper for the Beam EDM experiment is reported. The experiment is realized by the Neutron Group of the University of Bern and it will take place at the Institut Laue-Langevin (ILL) in Grenoble. The purpose of the Beam EDM experiment is to measure the neutron electric dipole moment using the separated oscillating field method (Ramsey method). Since a pulsed beam of cold neutrons needs to be produced for the experiment, a device is placed between the continuous beam of cold neutrons and the rest of the apparatus which is used for performing the Ramsey method. A chopper has been built for this reason.
The chopper has been realized with a collimator box in which a set of Silicon wafers are put in. The collimator box is placed on top of a rotating turntable: neutrons can pass through the chopper twice per revolution. The rotating plate is fixed on an aluminum structure and it is moved by a stepper motor. In order to monitor the rotation speed of the chopper, a system for measuring the frequency has been realized using an Arduino DUE microcontroller. A motor control box has been built with the Arduino micro-controller and a motor control board. On one side, the Arduino micro-controller sends commands to the motor control board, on the other side, it checks the chopper rotation frequency.
In this report, the description of the chopper mechanics and the realization of the electronics are reported. Moreover, several characterization tests are presented and discussed.

Chapter 2

Chopper system components

The chopper is a complex system which can be divided in electronics and mechanics. Both electronics and mechanics have been thought and built for the Beam EDM experiment. The electronics is based on the micro-controller Arduino DUE which drives the stepper motor, controls the rotation frequency of the chopper and communicates with the PC. The mechanics is composed by different aluminum parts and, at the center of the entire structure, the collimator is placed. In the following, the main components of the chopper are reported:

- stepper motor QSH6018-86-28-310 from TRINAMIC
- collimator box with Silicon wafers inside. Two different types of wafers have been produced for the collimator: Silicon wafers painted with a mixture of Gd_2O_3-powder and Silicon wafers with sputtered gadolinium
- aluminum support structure with an aluminum rotating plate for the collimator and the stepper motor
- two *BorAl* plates are placed on the sides of the in-coming and out-coming neutron beam, while three aluminum panels close the other two sides and the top of the chopper
- chopper control box with motor control board TMCM-1160 and Arduino DUE
- System for frequency measurement with laser and photodiode circuits.

Starting from the mechanics until the elements of the chopper electronics, all the components are described in this chapter.

2.1 Stepper motor

The stepper motor driving the chopper is the model QSH6018-86-28-310 from TRINAMIC. It contains two coils called A and B, each of which is powered via 2 pairs of wires. These 4 wires are connected to the TMCM-1160 which drives the power of the motor. The two coils allow the motor shaft to rotate by changing the polarity in two directions: clockwise and counter clockwise. The number of steps per turn is an intrinsic characteristic of the motor which is related to the coils and the mechanics of the motor. In this case, the number of steps per turn is equal to 200. Moreover, for each step, the motor can be moved by a maximum number of 256 microsteps. All the detailed properties of this stepper motor can be found in the manual available online on the website of TRINAMIC [1] . In the table 2.1, the main characteristics of the stepper motor are summarized.

Specifications	Units	Value
Weight (Mass)	kg	1.4
Motor length	mm	86.0
Axis diameter	mm	7.5
Axis length	mm	22.4
Max applicable voltage	V	75
Connection wires		4
Holding torque (typ)	N·m	3.1
Rotor inertia	g·cm^2	840
Full step resolution (number of steps per full rotation)		200
Step angle	degree	1.8
Step angle accuracy	%	5

Table 2.1: Table with the main characteristics of the stepper motor QSH6018-86-28-310. The information are taken from the TRINAMIC manual.

The torque of the motor depends on the rotation velocity. This dependency is shown in Figure 2.1, where the speed is reported in pulses (microsteps) per second (*pps*). This is related to the round per second (*rps*) through the following equation (eq. 2.1):

$$v_{rps} = \frac{v_{pps}}{r_{fullstep} \cdot r_{microstep}} \tag{2.1}$$

where v_{rps} is the motor velocity in *rps*, v_{pps} the velocity in *pps*, $r_{fullstep}$ the number of steps to obtain one round and $r_{microstep}$ the number of microsteps for every single step. The graph has been obtained in the full step configuration (no microsteps).

[1] *www.trinamic.com/products/drives/stepper-motors-details/qsh*6018/.

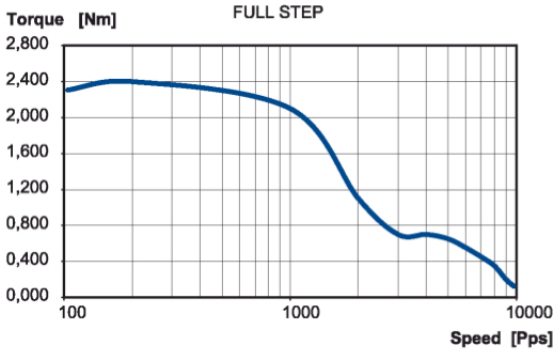

Figure 2.1: The motor torque as a function of the motor speed in pulse per second (*pps*) is represented. This measurement has been obtained in the full step configuration. The speed in *pps* is proportional to the rotation velocity of the motor (see eq. 2.1). The figure shows that the motor torque decreases for velocity above approximately 1000 *pps* equal to 5 Hz.

The torque that the stepper motor can apply results to be constant for velocity lower than approximately 1000 *pps* which is equal to 5 Hz. Above this velocity the torque decreases.

2.2 Chopper mechanics

The chopper mechanics is built in aluminum and it is composed by a base for the chopper, a rotating plate on top of which the collimator is placed and the bars used to keep aligned the rotation axis of the rotating plate. The schematic of the chopper mechanics is shown in Figure 2.2.

The picture 2.2 (a) shows a vertical section of the chopper. Starting from the bottom, the structure is composed by one aluminum profile 120x40 mm which sustains the aluminum base plate of the chopper. On top of the base plate a cylindrical piece is placed in central position which surrounds the stepper motor shaft and the rotating plate shaft. Inside the cylindrical piece, the two shafts are attached thanks to a brass clutch which allows the motor to move the rotating plate (point 3 of the Figure 2.2 (a)). The collimator box is installed and fixed with screws on the rotating plate, then it is secured by two vertical bars and one horizontal bar. The two vertical bars are screwed in the rotating plate in contact with the closed sides of the collimator box. The horizontal bar is fixed to the vertical bars and secures the box to the rotating plate. This horizontal bar is built with a shaft in its center which is inserted in the upper horizontal bar (point 14 of the Figure 2.2 (a)). This shaft needs to be precisely aligned with the center of the entire structure since it fixes the rotation axis of the chopper and avoids oscillations. The upper horizontal bar holds two lasers which are

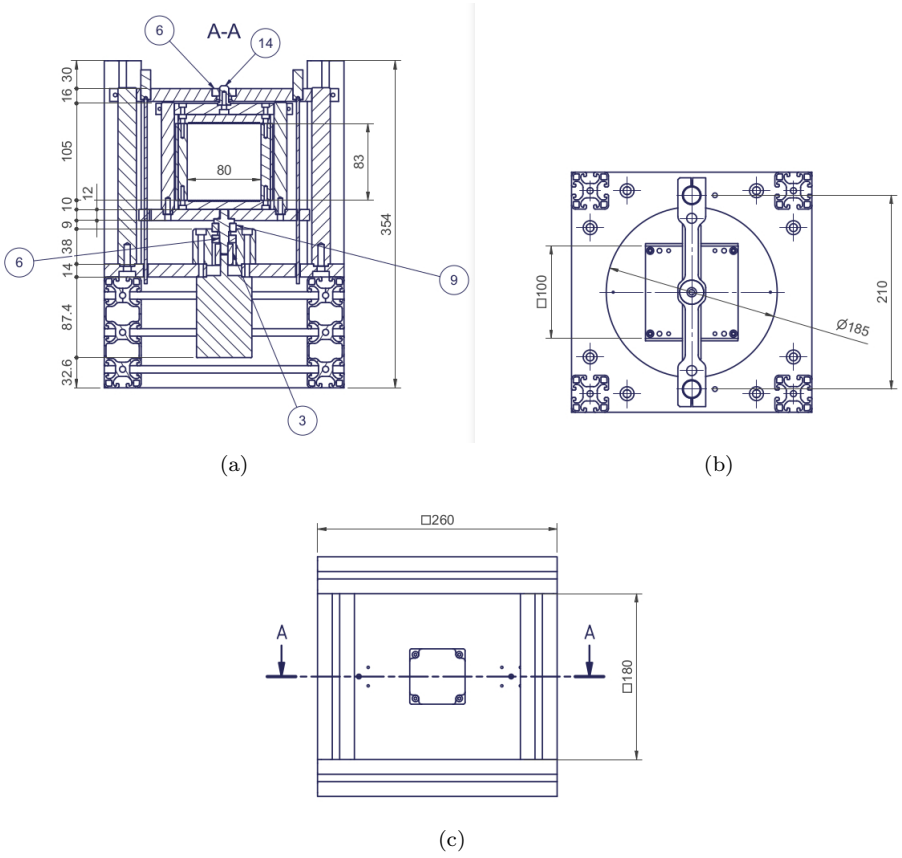

Figure 2.2: Design of the chopper with the wafers box installed on the rotating plate. In (a), a frontal section of the chopper is shown with the collimator box and the motor. In (b) the top view and in (c) the bottom view are presented. The two holes for the photodiodes can be seen in (c).

downward oriented. This bar is fixed to two vertical bars which are screwed in the base plate. To avoid any friction, stainless steel bearings are installed in point 4, 6 and 9 of the Figure 2.2 (a). In Figure 2.2 (b), a view from the top of the chopper is shown with the upper bar and the collimator on the rotating plate. The two lasers on the upper bar are placed at a different distance from the rotation axis: one is placed at 85 mm and the other one at 80 mm. In Figure 2.2 (c), the bottom of the base is shown. The stepper motor is attached in the center of the base plate and fixed to it with screws. The base plate is provided with one hole in the center where the motor shaft is inserted. Two other holes are provided on the axis A of the picture, which host the photodiodes. Each photodiode is soldered on a small PCB which is screwed in the base plate. The photodiodes holes are placed to a different distance from the center of the base

plate: one is at 85 mm and the other one is at 80 mm.

Four holes are provided on the rotating plate. They can be divided in two pairs of holes: one pair is aligned with one photodiode and one laser when the chopper is in the open position (Figure 2.3 (a)) and the second is aligned with the second photodiode and the second laser when the chopper is in the close position (Figure 2.3 (b)). The two pairs are shifted by 90° between each other and the distance from the center of the rotating plate for one pair is 80 mm and for the other is 85 mm.

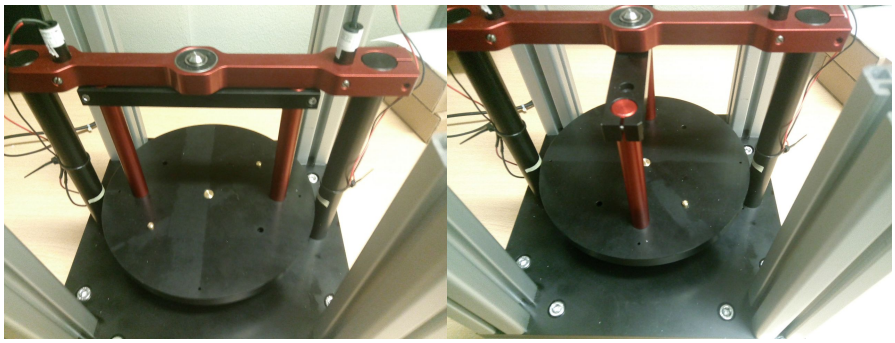

(a) (b)

Figure 2.3: Pictures of the chopper without the collimator box in open position (a) and in close position (b). In (a), the laser on the right is aligned with the right hole on the rotating plate. A second hole is made at 180° on the plate, in this way, the laser light hits the photodiode twice each turn: this allows to detect every time the chopper is in the open position. The same method is used for the close position. In (b), the left laser is aligned with the hole left hole when the chopper is closed. As before, a second hole is present on the plate at 180° with respect to the first.

Four vertical aluminum profiles are screwed in the base plate and they are used to fix five panels that close the chopper: one for each side and one for the top. The panels are made in aluminum except for the panels in the in-coming and out-coming beam direction which are made by neutron absorber material *BorAl*. The 3D-CAD drawings of the chopper are presented in Figure 2.4. The apertures for the in-coming and out-coming neutron beam on the *BorAl* panels can be adjusted and the beam dimension can be modified.

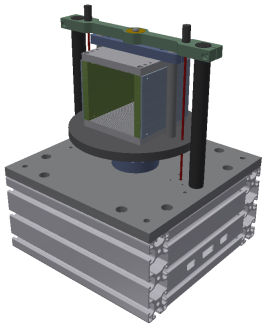

(a)

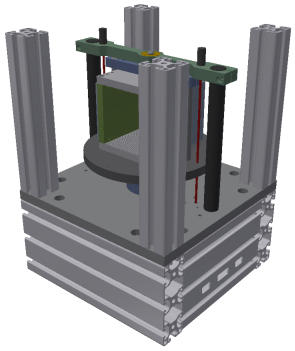

(b)

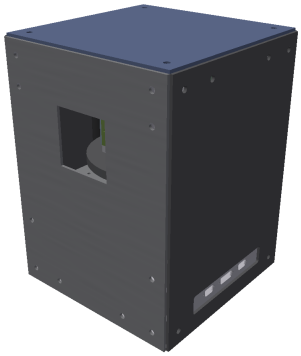

(c)

Figure 2.4: 3D CAD design of the chopper. Figure (a) shows the design of the chopper with the collimator box in the open position. In Figure (b) the four aluminum profiles have been added at the four angles of the chopper base plate. In Figure (c) the five panels have been mounted and fixed to the four profiles: the dimension of the square shape hole can be modified by adding a set of apertures in *BorAl*. The red lines in (a) and (b) represent the laser light.

2.2.1 Collimator box

The collimator box is made of a set of Silicon wafers. Two types of Silicon wafers have been produced: one type is a Silicon wafer coated with Gd_2O_3 0.8 mm thick and the second type is a Silicon wafer with gadolinium sputtered 0.4 mm thick. The Silicon wafers are placed in an aluminum box with a cross-section of 80×83 mm (inner sizes). Figure 2.5 shows the collimator box with the full set of Silicon wafers coated with Gd_2O_3. On the bottom side and on the top side of the box a set of slits is machined in which the wafers can be inserted. The two sides perpendicular to the wafers plane are open, while the two sides parallel to the wafers absorb neutrons thanks to the additional $BorAl$ plates attached to them. When the two open sides are aligned with the beam, the neutrons can pass through the chopper. In general, it is possible to determine a geometric angle which defines the open window of the chopper: two times per turn the chopper is open and the neutrons fly through. This geometric angle depends on the characteristics of the chopper, in particular on the distance between the wafers. In this setup, the center-to-center distance of the wafers can be adjusted in steps of 2 mm. A second version of the collimator box is available with a center-to-center distance of 5 mm.

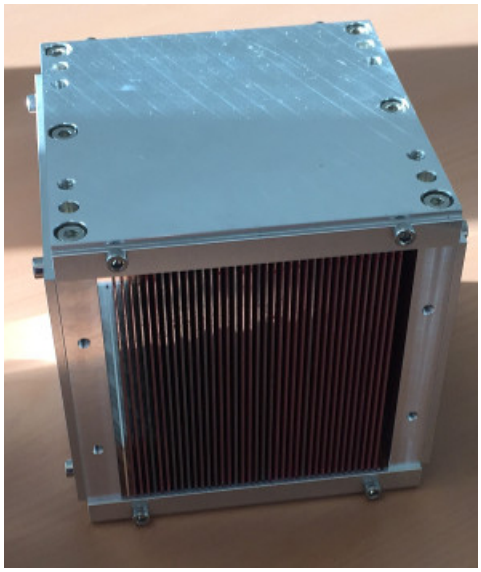

Figure 2.5: Picture of the collimator box with the full set of Silicon wafers coated with Gd_2O_3 inserted. In this version of the collimator box, the center-to-center distance between two wafers can be adjusted in steps of 2 mm.

2.3 Chopper Control box

A box has been realized in order to contain the motor control board TMCM-1160 and the system controller Arduino DUE. A picture of the motor control box is presented in Figure 2.6. The box is powered by an external power supply

(a) (b)

Figure 2.6: Pictures of the motor control box. In (a), the plug for the power supply and the RS-232 plug for the PC-Arduino connection are shown. Figure (b) shows the two D-sub 9 pins connectors for the photodiodes and lasers, the Sub-d 15 pins connector to control the motor and two LEMO plugs to readout the pulse from the photodiode in the open position.

with 24 V and 2.5 A. The box has a power-plug connector and a RS-232 plug for the connection with the PC on one side. After it has received a request, the box translates and sends the command to the motor. On the opposite side, the box is connected with the motor and the two laser-photodiode pairs respectively by means of a D-sub 15 pins connector and two D-sub 9 pins connectors. Moreover, two LEMO $4M$ plugs are provided on the same side where the signal from the photodiode in the open position can be directly read-out.

2.3.1 TMCM-1160

In order to control the stepper motor, the TMCM-1160 board is used. A set of commands is integrated in the board and translated to the motor (see TMCM-1160 firmware manual). There are three different ways to control the board: USB, CAN or RS-485 communication. Since the TMCM-1160 is controlled via Arduino, the RS-485 communication has been chosen. In Figure 2.7, a picture of the board is presented together with the connections scheme. The motor is connected and driven through the plug *JST B4B-EH-A* on the bottom of the figure: the black and green wires are connected to the motor coil A and the red and blue wires to the motor coil B (see TMCM-1160 hardware manual).
A +24 V/2.5 A input is supplied by an external power supply via the *JST B4B-EH-A* on the left of the figure: a short-cut connection is needed between the two central pins to enable the driver stage of the board. The maximum

input values for the current and the voltage that the TMCM-1160 can handle are +51 V/2.7 A.

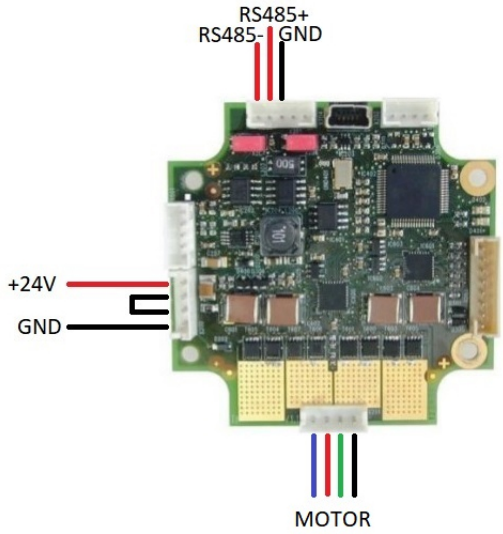

Figure 2.7: A picture of the TMCM-1160 motor control board produced by TRINAMIC is presented including the connections scheme.

The five pins connector *JST B5B-PH-K-S* on top of the picture is used for the serial communication. The chosen settings for the RS-485 communication is $8N1$: every command is made of 8 bits without parity and with 1 stop bit. The baudrate is set to 9600. The standard protocol for the command format is provided by TRINAMIC. Each command is composed by 9 bytes: the first byte indicates the module address, the second byte the command number, the third the type number, the fourth the motor number, then four bytes are dedicated to the value to be transmitted, while the last byte is the check sum[2].

[2]The check sum is equal to the sum of all the other bytes. When the command is received, if this byte is different from the sum, then the information is corrupted.

2.3.2 Arduino DUE

Arduino DUE plays a central role in the whole system, it is not only used to control the motor and to check its frequency, but it is the central node of all the communications related to the chopper. For this reason, it has been decided to realize a custom-made PCB that is installed on the Arduino DUE as shown in Figure 2.8 (a): pins are soldered on the circuit and are connected with the Arduino pins. The black metallic piece on top is used as cooling plate for the voltage regulator $LM7812$ which supplies the Arduino: the input of +24 V from the external power supply is reduced to +12 V. The output of the regulator is connected to the Arduino V_{in} pin[3]. A 2200 μF electrolytic capacitor is soldered in between the ground and the input voltage of the regulator to reduce the noise from the power supply. Figure 2.8 (b) presents the schematic of the main connections: RS-232, RS-485 and photodiodes connections.

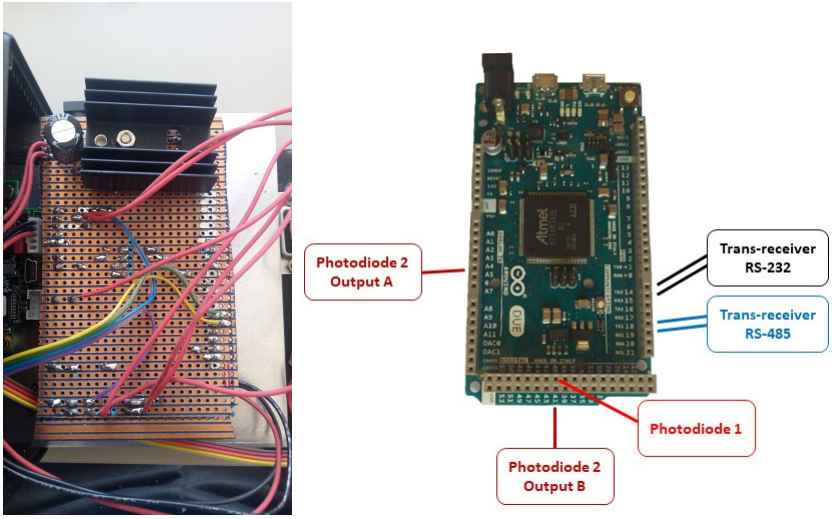

(a) (b)

Figure 2.8: A picture of the Arduino DUE and a schematic of the main connections are shown. In figure (a), a picture of the custom-made PCB installed on the Arduino is presented. On the top of the picture, a heat absorber for the voltage regulator can be seen close to an electrolytic capacitor. In figure (b), the connection scheme of the Arduino DUE is reported.

Every request sent from the PC via RS-232 to the chopper is processed by the micro-controller. Then, if there is a command direct to the motor, this is translated in the standard protocol and sent to the TMCM-1160 via RS-485. The protocol used for the data transmission between the PC and Arduino is

[3]the maximum input voltage for this pin is equal to 12 V, higher voltage could damage the board.

$8N1$ with a baud rate of 115200. The command format is made of 9 bytes and it is similar to the TMCM-1160 standard format. In order to communicate via serial, the Arduino micro-controller needs a trans-receiver chip to convert the TTL signal to serial logic levels. For this reason, a MAX3232 board is used for the RS-232 communication with the PC. The RX and TX are respectively connected with the RX3 and TX3 pins of the Arduino board. The MAX3232 board is based on the $MAX232$ chip which is powered by the Arduino with +5 V.

For the same reason, the RS-485 communication between Arduino and the TMCM-1160 board has been established using another trans-receiver chip: the $MAX485$. In this case the circuit has been soldered on the custom-made PCB. The detailed schematic of the circuit for the MAX485 circuit is shown in Figure 2.9.The pin RO and the pin DI are connected to the Arduino pins RX1 and TX1. The driver enable DE and receiver enable RE are driven by Arduino respectively with pins 4 and 5: RE is set in high impedance state (pin 5 is HIGH) and DE is set at 0 V (pin 4 is LOW) when Arduino is sending data and viceversa when the Arduino is receiving. The circuit is supplied by the Arduino with +5 V. The Arduino is also used to read the signal from the photodiodes.

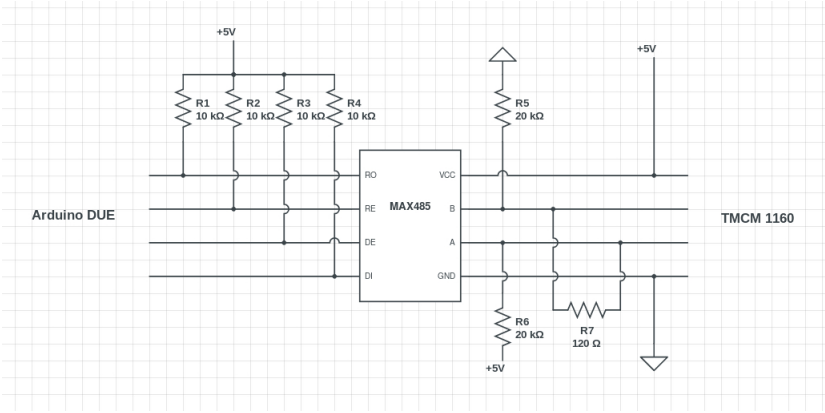

Figure 2.9: Schematic of the MAX485 circuit for the RS-485 serial communication. The pin RO is connected to the pin RX1 of the Arduino, while the pin DI is connected to the pin TX1. The driver enable DE and receiver enable RE are driven by the Arduino respectively with pins 4 and 5. The A and B lines are the respectively $RS485+$ and $RS485-$ which are connected with the TMCM-1160. The MAX485 operates at +5 V.

As shown in Figure 2.8 (b), the pin A5 is connected to the output A of the photodiode circuit (Photodiode 2) which is triggered when the chopper is in the open position. This pin is used to find the open position of the chopper: the chopper is moved microstep by microstep until the laser light hits the photodiode and the input on A5 is HIGH. The signal comes from the comparator (output A

of Photodiode 2). A second output is given from the monostable (output B)[4]. The pulse from this output is received in the pin 41 and it is used to calculate the relative time between two consecutive pulse. The signal from output B is the same signal that can be read out with the two LEMO plugs on the box.
The pin 40 is connected to the other photodiode circuit (Photodiode 1), which is triggered when the chopper is in the close position. In this case there is only one output and it comes from the comparator.

[4] A Monostable Multivibrator is an operational amplifier which has only two different output states: one is stable and the other one is unstable. The output is always in the stable state, however, if the monostable is triggered by an external input, the output switches from the stable state to the unstable state for a set period of time. This time period is defined by the components of the circuit.

2.4 Photodiode circuits

In order to monitor the rotation frequency and find the position of the chopper, two downward oriented lasers are installed on the upper bar of the chopper (Figure 2.5). These two lasers are aligned with two photodiode circuits attached to the chopper base plate. While the chopper is turning, the four holes on the rotating plate allow to trigger one photodiode circuit when the chopper is in the close position (Photodiode 1) and the second photodiode circuit when the chopper is in the open position (Photodiode 2). Each circuit is triggered twice per revolution. The laser model is TIM-201-5D/650 and it is connected to the pin +5 V of Arduino.
The Photodiode 1 is hit by the laser when the chopper is in the close position. The output of the photodiode is connected to the non-inverting input of a comparator which generates a square shape pulse. The length of this pulse is equal to the exposure time of the photodiode to the laser light. For this reason, the output signal can be parametrized as HIGH (+5 V) if the laser light hits the photodiode, otherwise LOW (0 V). The output value of +5 V is due to the operative voltage supplied to the comparator. The operational amplifier used as comparator is the ADCMP601. In Figure 2.10, the detailed schematics of the circuit and the components values are reported.

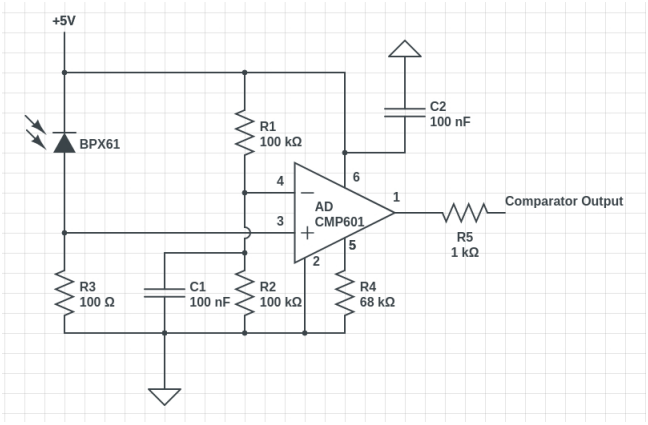

Figure 2.10: Schematic of the comparator circuit with ADCMP601 amplifier. The values of the components are reported.

The laser hits the Photodiode 2 when the chopper is aligned with the beam direction. The signal from the photodiode is processed by the same comparator stage shown in Figure 2.10, but an additional stage is present. In fact, the output of the ADCMP601 is connected to the input of the monostable 74HC123N. The additional monostable stage gives a +5 V square pulse of 1 ms long when the chopper is in the open position. The length is defined by the value of the capacitor and resistor pair connected to the pins 14 and 15. The entire schematic

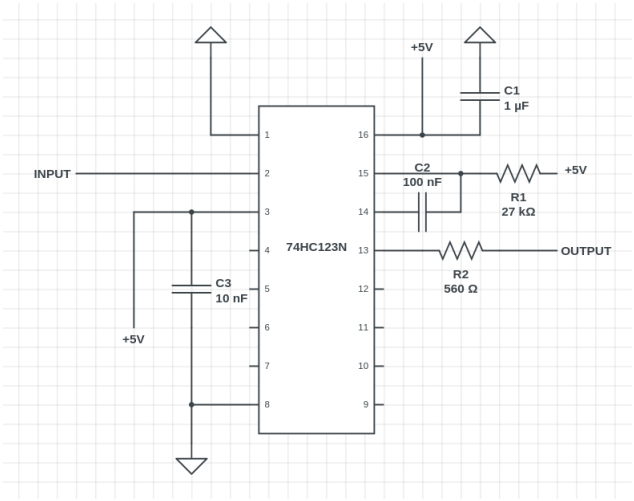

Figure 2.11: Schematic of the circuit used to measure the frequency. The comparator stage output is connected to the monostable stage input. The final output is a square waveform with a length of 1 ms.

of the monostable circuit is represented in Figure 2.11. Two output signals are taken from the Photodiode 2: the output signal from the comparator stage (output A) and the output signal from the monostable (output B). The signal from the output A is used to find the open position of the chopper, while, the signal from output B is used to measure the rotation frequency of the chopper and as trigger signal for the detector of the experiment.

In Figure 2.12 (a) a picture of the circuit Photodiode 2 is reported. The photodiode is placed at the center of the PCB, while the comparator (white chip) can be seen on the left top part of the board. The monostable is the black chip on the right side of the board. An example of the output signal from the monostable is shown in Figure 2.12 (b): the exact length is 1.02 ms. Two sources of noise have been found which needed to be eliminated. The first was the external power supply and the second was due to the contact between the circuits and the base plate. The external power supply generates a peak-to-peak noise of 120 mV, this value has been reduced to $\sim$ 30 mV thanks to the 2200 μF capacitor placed between +24 V and the ground. The two circuits are screwed in the bottom part of the base plate very close to the stepper motor. At the beginning, the screws used to fix the circuits were metallic, but this caused an electric contact between the base plate and the photodiode circuits. Moreover, the chopper base plate was in contact with the top of the motor. For this reason, the output signal from both the circuits was disturbed by noise. However, the metallic screws have been replaced with nylon screws and the noise disappeared.

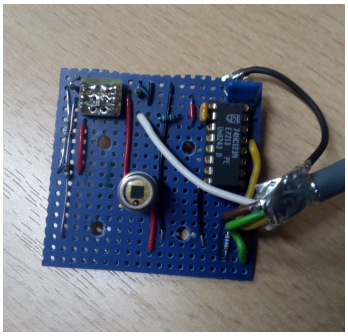

(a)

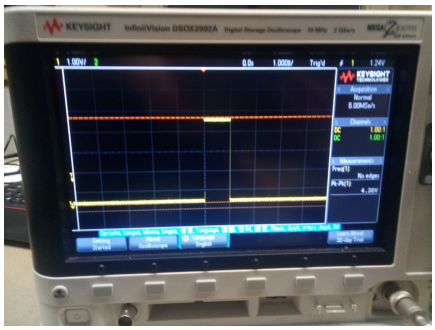

(b)

Figure 2.12: Picture of the photodiode circuit in (a) and its generated signal at the oscilloscope in (b).

Another problem was due to the interference of the motor and the circuits. To solve this problem, two metallic boxes and shielded cables have been used to shield the circuits and to avoid any interferences. In Figure 2.13, a picture of the bottom of the chopper with the stepper motor and the two boxes with the photodiode circuits is shown.

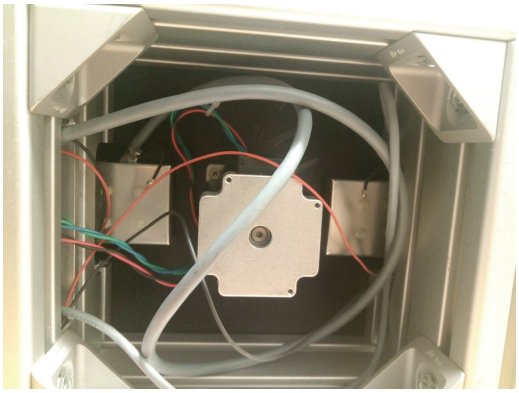

Figure 2.13: Picture of the bottom of the chopper. The stepper motor with the two metallic boxes containing the photodiode circuits can be seen.

2.5 Cables

In order to connect the motor and the photodiode circuits to the control box, three 10 meters long cables have been realized. A picture of the cables is shown in Figure 2.14.

Figure 2.14: Picture of the cables realized to connect the motor and the circuits to the motor control box.

The black cable with D-sub 15 pins connector connects the motor control box with the motor: the two pins pairs (1,2) and (3,4) are connected to coil B, while (5,6) and (7,8) are connected to coil A.
The two grey cables are completely interchangeable. They are used to supply the two photodiode circuits and the two lasers. For this reason, pins (1,2) are connected to +5 V, pin 3 is connected to the output signal (comparator output for Photodiode 1, monostable output B for Photodiode 2), pins (4,5) are connected to the ground. Pin 7 is used only with the Photodiode 2 circuit and it is connected to the output A (comparator).

Chapter 3

Chopper characterization

Several test have been performed with the chopper. In particular, the photodiode circuits test, the mechanics stability of the chopper and a test on neutron beam at ILL in Grenoble are discussed in this chapter.
The reliability of the photodiode circuits is fundamental, in fact, as already discussed in the previous chapter, one circuit is used to find the close position of the chopper (Photodiode 1) and the second one is used to find the open position (Photodiode 2): the chopper turns microstep per microstep until the laser light hits the circuit and it is important that the photodiode is always triggered by the laser light and signal is processed by the operational amplifiers. Moreover, the signal from the Photodiode 2 is used to measure the rotation frequency of the chopper and it is the trigger signal for the detector: this implies that every time the chopper is open, exactly one pulse must be generated.
Since the chopper will be running for several weeks, it is important to test its mechanics stability together with the performances of the stepper motor over the time.
In the end, a test with neutrons at ILL has been performed in order to characterize the chopper. The Silicon wafers have been characterized and a time-of-flight measurements have been performed. The results of all these tests are reported and discussed in this chapter.

3.1 Photodiode circuit stability test

It is crucial for the whole experiment that the circuit in the chopper open position converts every pulses from the laser into a square shape waveform of 1 ms length. For this reason, the number of pulses has been counted at a set frequency of 10 Hz. The time difference between two consecutive pulses has been measured for more than 14 hours.
In order to perform this test, the square shape pulse is analyzed by connecting the LEMO plug on the motor control box with the National Instrument multifunction DAQ 6363. The data is saved on PC thanks to a LabView program.

For each pulse, an absolute time, a counter and the time difference with the previous pulse have been recorded. The expected result is a straight line with the delta time value equal to 0.05 s (i.e. 20 Hz). In fact, since two holes are present on the rotating plate, the measured frequency is double the value of the set frequency.

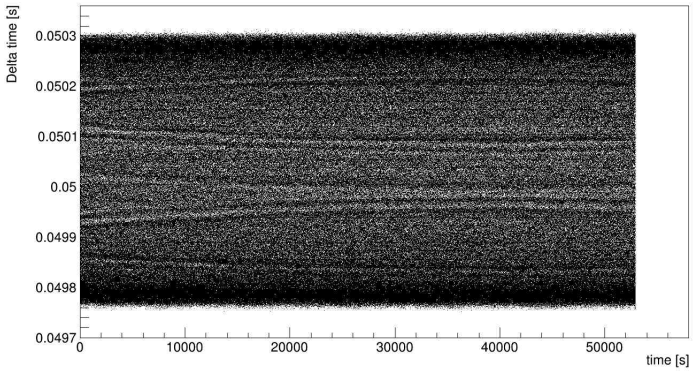

Figure 3.1: Time difference between two consecutive pulses as a function of the acquisition time.

The result of the measurements is shown in Figure 3.1. The measured frequency is not exactly equal to 20 Hz, but no pulses are missing and there are no double counts, otherwise, there would be points outside the band.

3.2 Chopper stability test

The chopper is supposed to work at different frequencies during the experiment for a long time. For this reason, a good stability at different rotation speed is required.
In order to investigate the chopper stability, the frequency has been measured over the time at different frequencies. The distribution of the measured frequency is expected to be a gaussian centered in the double the value of the set frequency, however, as can be seen in Figure 3.2, the obtained distribution is not a gaussian. This histogram is obtained from the stability measurement at 10 Hz of the photodiode circuit (Figure 3.1). The distribution is centered around 20 Hz as expected, however, two peaks are present at the two edges of the distribution. The shape of this distribution has been studied and compared with the same measurements at lower and higher frequencies.

In particular at frequencies lower than 6 Hz, the distribution has a guassian shape as can be seen in Figure 3.3 where the distributions obtained at 3 Hz and 5 Hz are shown. This shape is completely different from the one obtained at higher frequency. In fact, for frequencies higher than 6 Hz, the double peaked

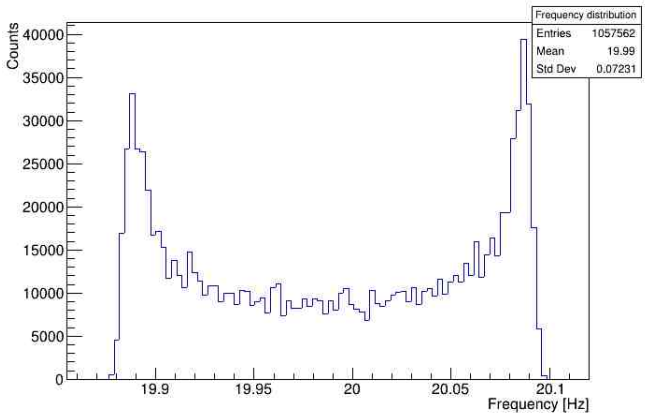

Figure 3.2: Frequency histogram obtained from the long term measurement shown in Figure 3.1.

distribution appears. This effect could be due to the less torque that the stepper motor applies above around 5.5 Hz as shown in Figure 2.1.

The measurement has been repeated at higher frequencies and the Amplitude of each distribution has been calculated as in 3.1:

$$Amplitude = \Delta t_{max} - \Delta t_{min} \tag{3.1}$$

where Δt_{max} and Δt_{min} are, respectively, the highest and the lowest values of the time difference between two consecutive pulses. The first set of measurements has been performed without the collimator box. Three different steps resolution have been studied to check if the amplitude depends on the number of microsteps of the motor:

- 128 microsteps per single step: frequency scan from 6 Hz to 15 Hz with 0.1 Hz step.
- 64 microsteps per single step: frequency scan from 5.5 Hz to 14 Hz with 0.5 Hz step.
- 256 microsteps per single step from 6 Hz to 9 Hz. In this configuration the motor maximum frequency is limited to 9 Hz.

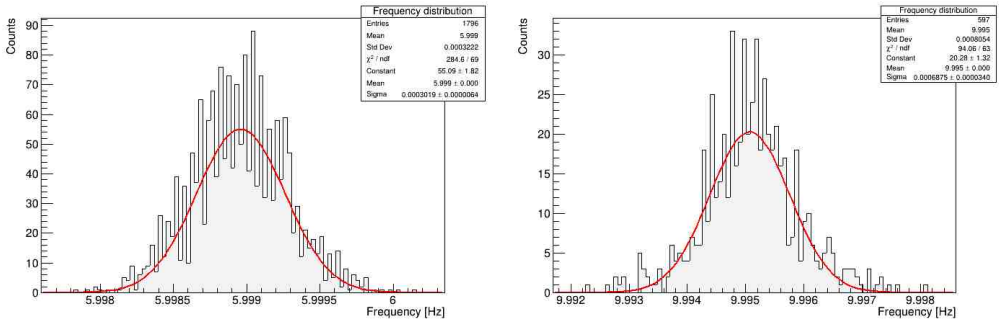

(a) 3 Hz (b) 5 Hz

Figure 3.3: Frequency distributions at 3 Hz in (a) and at 5 Hz in (b). A gaussian fit has been performed.

The results from these three different measurements are reported in Figure 3.4. The lowest amplitude is obtained at around 7.8 Hz for the three configurations, this implies that the amplitude does not depend on the microstep resolution.

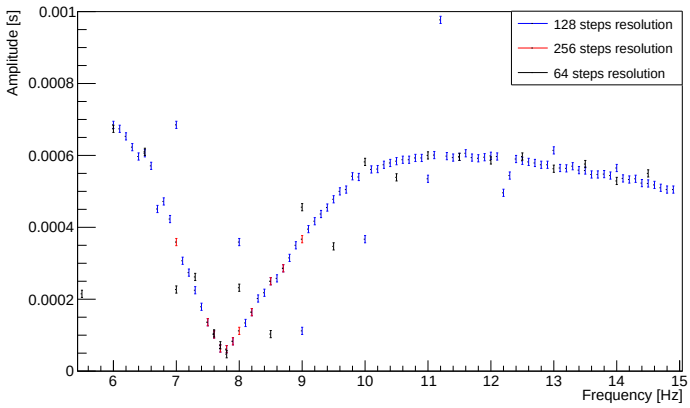

Figure 3.4: Frequency distribution amplitude as a function of the frequency. The plot has been obtained with three different microstep resolution: the red points are obtained with 256 microsteps per step, the blue points with 128 microsteps and the black points with 64 microsteps. The amplitude of the frequency distribution reaches its minimum around 7.8 Hz.

Resonances can be observed at different frequencies. An example of this is shown in Figure 3.5 where the time difference between two consecutive pulses (Delta time) as a function of the acquisition time is reported for the measurement at 12.1 Hz.

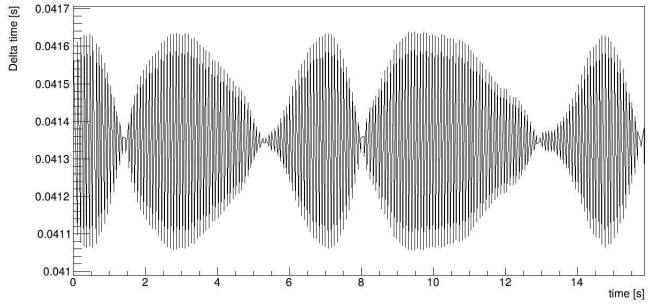

Figure 3.5: Plot of time difference between two pulses as a function of the acquisition time: first 15 seconds of the measurement at 12.1 Hz.

After these measurements, the collimator box has been installed on the rotating plate and the measurement with 128 microsteps resolution has been repeated in the range between 5 Hz and 14 Hz. In particular, the frequencies close to 7.8 Hz have been the focus of this measurement. In Figure 3.6, the result is shown and compared with the previous measurement. The amplitude minimum is found at lower frequency ($\sim$ 6.4 Hz): the two distributions are similar, but the black is shifted left compared to the blue. The two different minima show a relation between the amplitude of the frequency distribution and the weight of the rotating plate.

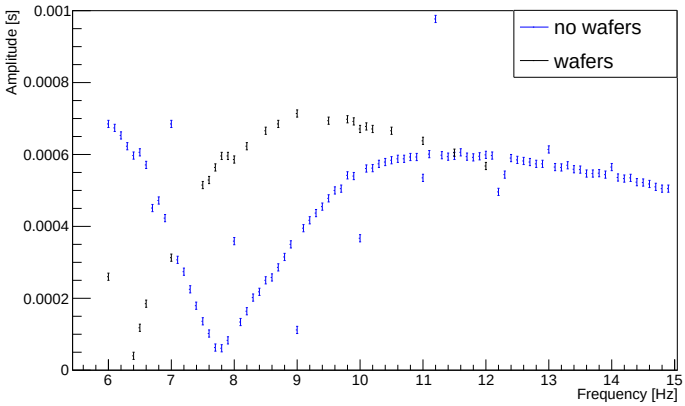

Figure 3.6: Time distribution amplitude as a function of the frequency: in blue the result obtained without the collimator box, in black with the collimator box. Two different minima are obtained.

3.3 Beam time at ILL

On February 20th and 21st, 2020, a test beam has been performed in Grenoble at ILL with the chopper. This test has been necessary to study and to characterize the chopper for the first time with neutrons.
In order to characterize the collimator, the properties of two different types of Silicon wafers have been studied. One type of Silicon wafers is 0.8 mm thick and it is coated with Gd_2O_3-powder, while the second type is a Silicon wafer 0.4 mm thick with sputtered gadolinium. To study the neutron absorption capability, each wafer has been placed on a support over a mechanical arm which was moved by a motor. Once the wafer was fixed on the support, a laser was used to center the neutron beam. Behind the wafer, a ^{3}He neutron detector was placed to determine the neutrons count.
The expected intensity after the wafer depends on the crossed material and it is given by the following equation 3.2:

$$I = I_0 e^{-\frac{\epsilon\lambda}{\lambda_0 \sin\theta}} \tag{3.2}$$

where I is the beam intensity after the wafer, I_0 is the beam intensity without the wafer, λ is the neutron wavelength, θ is the angle between the wafer plane and the beam direction and ϵ is related to the thickness of the absorption layer and to the density of the absorber. The ϵ parameter has to be determined.
The full intensity of the neutron beam has been measured by removing all the material on the neutron beam path to the detector and a total number of 2394×10^5 has been counted after 60 s. The background has been measured using a very strong neutron absorber: a Cadmium foil. After 60 s, a total

number of 341 neutrons has been counted.
After these preliminary measurements, each wafer has been characterized by varying the angle between the neutron beam and the plane defined by the wafer. Initially, the wafer was perpendicular to the neutron beam (90°), then by moving of 1° steps, it reached an angle of 158°: the measurement time for each angle is 4 s.

Figure 3.7 shows two examples of this measurement. The measurement with a Silicon wafer coated with Gd_2O_3-powder and the measurement with a Silicon wafer with gadolinium sputtered are reported respectively in (a) and in (b). The fit (in red) is performed with the equation 3.2 where ϵ and I_0 are the free parameters.

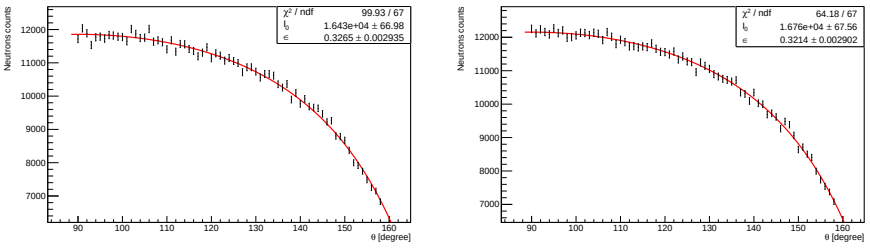

(a) (b)

Figure 3.7: Neutron total counts as a function of the angle θ: in (a) and in (b) are respectively shown the measurement with a Silicon wafer coated with Gd_2O_3-powder and the measurement with a Silicon wafer with gadolinium sputtered. The graphs are fitted with the equation 3.2: the only free parameters is ϵ, while $\lambda/\lambda_0 = 1$.

As expected, the fit is consistent with the data and the number of neutrons decreases as θ increases, in fact, the effective length of the wafer increases. Due to the different thickness between the two types of wafers, the absorption is expected to be better for the thicker wafer. However, there is a small difference between the two. This measurement has been repeated for the full set of wafers. In order to see the variation of the neutrons counts with the thickness, two and then four gadolinium sputtered wafers have been placed together between the continuous beam and the detector. Figure 3.8 shows in (a) the measurement with two wafers, while (b) the measurement with four. The fitted value of the ϵ are two and three times the value obtained with one gadolinium sputtered wafer. With the equal thickness, the absorption obtained with the gadolinium sputtered wafer is better than the wafer coated with Gd_2O_3-powder.

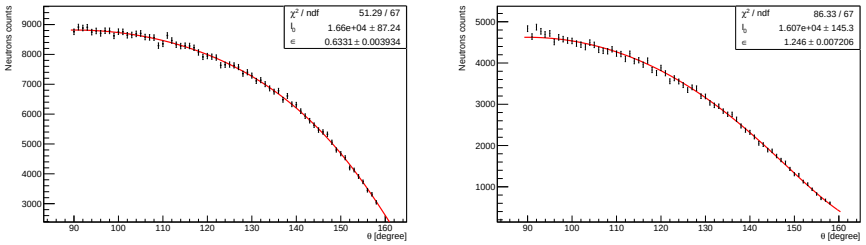

(a) (b)

Figure 3.8: Plots of neutron counts as a function of the angle: the plot (a) is obtained with two wafers, the plot (b) is obtained with four wafers. The fits of the two data set are reported in red.

3.3.1 Time of flight measurements

After the characterization of the wafers, the chopper has been assembled and installed at PF1B to perform a time of flight measurement. The Silicon wafers coated with Gd_2O_3-powder have been used for this measurement with a center-to-center distance between two wafers of 2 mm. The chopper has been placed at the end of the neutron guide and the ^{3}He detector has been placed at a distance of 1.70 m from the chopper. The aperture of the chopper on the in-coming beam and on the out-coming beam have been set at 40×30 mm^2.

Two measurements have been performed at two different frequencies: one with the chopper rotating at 7.5 Hz and the second one at 15 Hz. For both, the measurement time has been 1000 s.

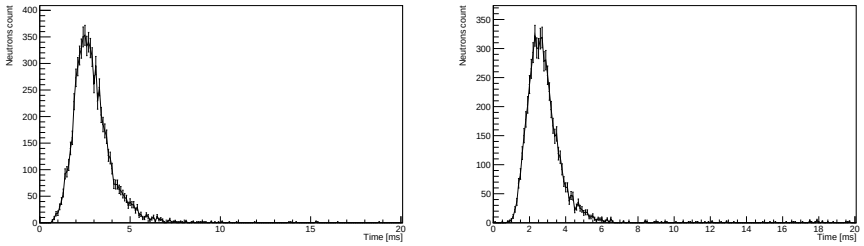

(a) (b)

Figure 3.9: Time of flight measurements with the chopper rotating at 7.5 Hz in (a) and at 15 Hz in (b).

The two measurements are shown in Figure 3.9: in (a) the measurement

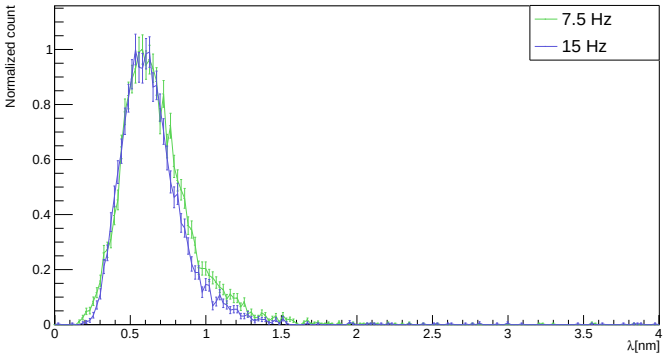

Figure 3.10: Neutron wavelength distributions obtained from the time of flight measurements. The distribution in green is obtained from the measurement with the chopper rotating at 7.5 Hz, while the blue distribution from the measurement at 15 Hz. As expected the two distributions overlap. The peaks are shifted with respect to the expected value which is for PF1B equal to $0.4 - 0.45$ nm.

with the chopper rotating at 7.5 Hz, while in (b) at 15 Hz.

The neutron wavelength λ and the neutron velocity v are related by the de Broglie equation 3.3

$$\lambda = \frac{h}{mv} \tag{3.3}$$

where h is the Planck constant, m the mass of the neutron. Considering the measure of the time of flight of neutrons over a given distance, it is possible to calculate the wavelength and measure the neutron spectra from the equation 3.3, as shown in equation 3.4:

$$t = \frac{\lambda L}{0.395} \tag{3.4}$$

where t is the time of flight of the neutron in milliseconds, L is the distance between the chopper and the detector in meters and λ is in nanometers. Figure 3.10 shows the wavelength distributions obtained with the de Broglie relation 3.4.

The mean wavelength for the neutrons at PF1B is expected to be around $\lambda \simeq 0.4 - 0.45$ nm, however the peaks of the distribution show a small shift to higher wavelengths. In fact, the two distributions peak at around 0.6 nm.

3.4 Input voltage test

After the test at ILL, an improvement of the performance of the chopper has been investigated. In particular, the goal was to improve the torque moment of the stepper motor by increasing the input voltage. The external power supply has been substituted with a Keysight E3630 power supply.
Unfortunately, the maximum input voltage that could be supplied to the voltage regulator used for the Arduino DUE was limited to +35 V. For this reason, the voltage regulator has been substituted with a Traco Power Supply THL 20-4812WI (Figure **??**). The input voltage range for this device is $18 - 75$ V, while the output voltage is +12 V and the output current is 1670 mA. The Traco Power Supply has two input pins where the ground and positive voltage are connected, and two output pins (ground and +12 V). A galvanic isolation is present between the input and the output of the Traco Power Supply (the current is not allowed to flow from the input to the output and viceversa).

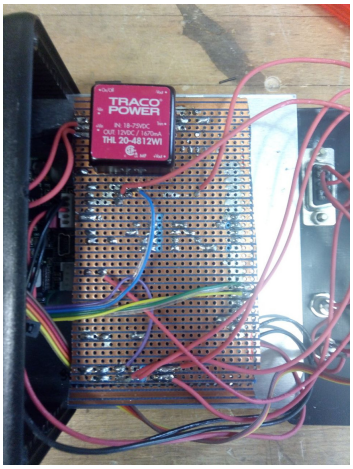

Figure 3.11: Picture of the Arduino DUE with the PCB on it and the Traco Power Supply.

As seen in the previous chapter, the frequency distribution is not always gaussian, for this reason the Amplitude of the distribution of the time difference between two consecutive pulses has been calculated as in 3.1. The goal has been to find the best configuration in which the amplitude is minimum.
As first test, different frequency scans have been performed by varying the input voltages with the Keysight power supply: 12 V, 24 V, 30 V and 50 V. These scans have been performed without the collimator.

In Figure 3.12, the plots of the frequency scans are shown. The Amplitude as a function of the chopper rotation frequency is reported for every input voltage. The red line represents the measurement obtained with the input voltage of 12 V, the blue line shows the measurement with 24 V, while the green line and the

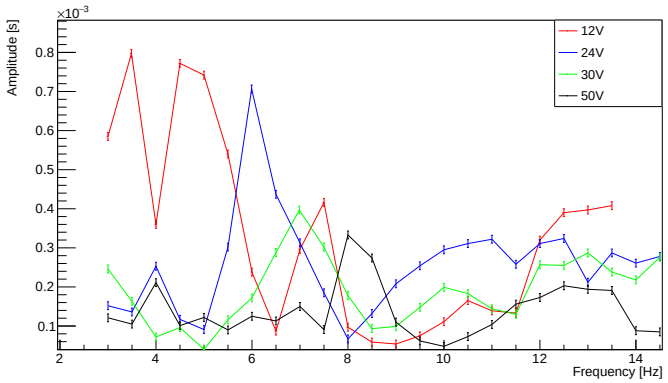

Figure 3.12: Plots of the Amplitude of the time difference between two consecutive pulses distribution as a function of the frequency. The measurements here reported are obtained with different input voltage supplied by a Keysight power supply. In red, the amplitude curve obtained with 12 V input, in blue the curve obtained with 24 V input, in green, the curve obtained with 30 V input and, in black, the curve with 50 V input. The chopper stability improves as the input voltage increases: at 50 V only one peak can be found compared to the several peak found at 12 V and 24 V.

black line represent the measurements, respectively, with 30 V and 50 V. It is clear from the plot that increasing the input voltage, increases the performance of the stepper motor and makes the rotation more stable. In fact, less oscillations can be found with the 50 V input compared to the lower voltages.
The stability of the chopper has been investigated by studying the variation of the amplitude with different configurations in which the weight of the chopper changes. The frequencies range studied starts from 2 Hz up to 14 Hz in steps of 0.5 Hz. The three main configurations tested are:

- Collimator: the collimator box introduces an additional weight on the rotating plate of around 1.4 kg. This is expected to improve the stability of the rotation
- Aluminum panels: with the aluminum panels mounted on each side, the chopper results to be heavier which is expected to deaden the vibrations during the rotation
- Lead bricks on top of the chopper: together with the aluminum panels this increases the weight of the chopper and this is expected to be helpful against the vibrations

In Figure 3.13, all the results from the frequency scans are shown: the Amplitude is reported as a function of the frequency and the three new measurements

are compared with the measurement obtained with 50 V (black line). The blue line represents the measurement with the collimator box on the rotating plate, the green line is the measurement with the aluminum panels, while the red line is the measurement with the two lead bricks.
An improvement in the stability is shown after the installation of the collimator box, in fact, the Amplitude is lower with the new measurements. Moreover, the peak at 8 Hz disappears completely after the installation of the collimator. In particular, the presence of the lead bricks on top of the chopper seems to stabilize its rotation, in fact, there are no more resonances at 6 Hz. Unfortunately, there is a small peak at 9 Hz in all the three new measurements.

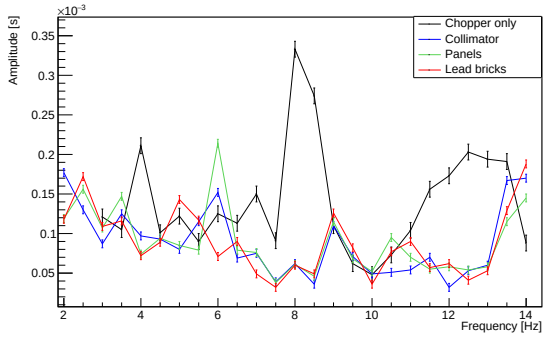

Figure 3.13: Amplitude as a function of the chopper rotation frequency for different frequency scans. The black line represents the measurement of the amplitude with the chopper with only the rotating plate without the collimator and the aluminum panels (see Figure 3.12). The blue line represents the measurement with the collimator over the rotating plate. The green line shows the measurement with the collimator and after the assembling of the aluminum panels at each side of the chopper. The red line is the measurement with two lead bricks over the top aluminum panel of the chopper. After installing the collimator, the peak at 8 Hz disappears. The lead bricks on top of the chopper improves the stability of the chopper, in fact, the measurement with only the panels shows a peak at 6 Hz which is deadened. A small resonance at 9 Hz is present in the three new measurements.

3.5 Chopper stability improvement

To reduce the vibrations during the rotation and to ensure a better stability to the rotation axis of the chopper at all the frequencies, a modification of the chopper design has been thought. The upper bar which holds the lasers and stabilizes the axis of the rotating plate, has been substituted with a completely new part. Four vertical bars have been installed on the base plate of the chopper to hold the new part and reduce the vibrations. All these new parts are shown in Figure 3.14.

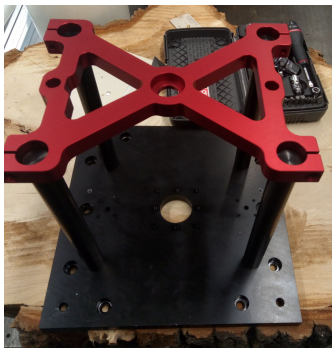

Figure 3.14: Picture of the new parts of the chopper. The upper bar has been substituted with the red piece in the picture. Four vertical bars have been installed on the base plate to hold the red part. This new design improves not only the stability of the chopper during the rotation by reducing the vibrations, but improves the stability of the laser during the frequency measurement.

In order to study the improvements introduced with the new design of the chopper, all the frequency scans previously performed have been repeated. The new amplitudes have been plotted together with the previous results in Figure 3.15 where the new measurements are represented in brown and the old measurement in blue. Figure 3.15 (a) shows the measurement obtained with the collimator box installed on the rotating plate. The resonance at 6 Hz disappeared with the new design, however a new narrower peak appeared at 5 Hz. The stability of the chopper has slightly improved in the range between 7 Hz and 13 Hz where the values of the amplitude are less spread than before. In Figure 3.15 (b), the measurements with the aluminum panels are shown: as before the amplitude values are similar between each other and the spread is reduced for frequencies below 13.5 Hz. At 13.5 Hz, the presence of a resonance increases the amplitude. In Figure 3.15 (c) where the measurements with the lead bricks on top of the chopper are reported, the new design shows still a slight improvement in chopper performances for frequencies below 11 Hz. For higher frequencies, an increase of the amplitude can be noticed which cannot be found in the measurement with the old design. The two lead bricks are not dampening the vibrations with their weight, but they introduce a new resonance.

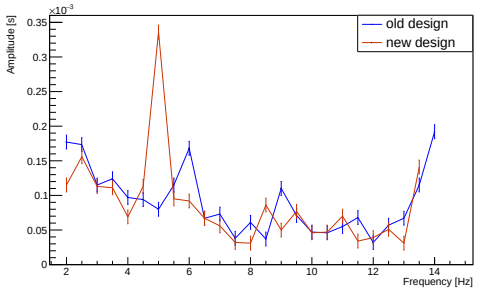

(a) Collimator box

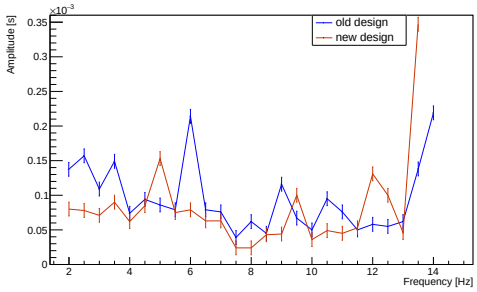

(b) Aluminum panels

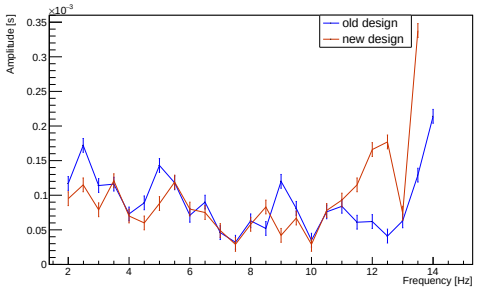

(c) Lead bricks

Figure 3.15: Graphs of the Amplitude as a function of the frequency. The measurement with the old design are represented in blue, while the measurement with the new design in brown. Figure (a) shows the two measurements with the collimator on top of the rotating plate. The amplitude is lower with the new design except for a new small resonance at 5 Hz. Figure (b) shows the measurements with the collimator and the aluminum panels mounted on each side of the chopper. Also in this case, there is a small improvement in the amplitude with the new design. Figure (c) shows the measurements with two lead bricks on top of the aluminum plate of the chopper. The weight of the two bricks for the new design is not as helpful as for the old design. In fact, the amplitude above 11 Hz increases.

Since the Amplitude of the distribution of the time difference between two consecutive pulses is related to the rising time of the trigger signal, it is important that the chopper rotates at those frequencies in which the amplitude value is minimum. In fact, for high amplitudes values, an error is introduced on the determination of the open window of the chopper. Considering the opening time τ of the chopper, this depends on the characteristics of the collimator box

and it can be calculated as following (equation 3.5):

$$\tau = \frac{d}{2\pi L}\frac{1}{f} \tag{3.5}$$

where d is the distance between two wafers, f is rotation frequency of the chopper and L is length of the wafers. In our case, d is equal to 5 mm and L is 100 mm. In Figure 3.16, the comparison of the measurements with and without the lead bricks is shown. The red line represent the values of the theoretical opening time calculated with the equation 3.5. The two lead bricks on top of the chopper introduce a small instability for frequencies higher than 10 Hz and the amplitude values obtained without them results to be more stable.

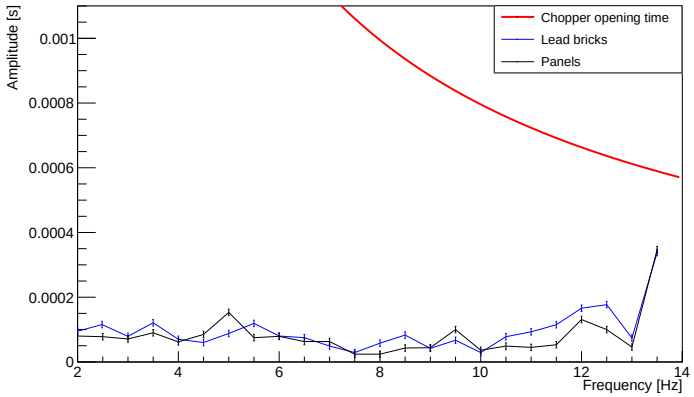

Figure 3.16: Graph of the Amplitude as a function of the frequency. The black line represents the measurement with the two lead bricks on top of the chopper, while the blue line is the measurement without the bricks. The red line is the theoretical opening time of the chopper calculated with the eq. 3.5. The goal is to obtain the lowest amplitude possible for all the frequencies. The black line show a slight better result compared to the black line for frequencies higher than 10 Hz.

Chapter 4

Conclusion

A new chopper has been thought and realized to generate a pulsed neutron beam for the Beam EDM experiment. Several tests have been performed to prove the reliability of every single parts of the chopper before the experiment. The electronics components are able to communicate with any external device that can control the chopper. The frequency monitor system has been tested and it is able to generate the trigger signal for the other devices of the experiment. A new design of the chopper has been realized in order to improve its stability and its performances. Among all the different tested configurations, the chopper has shown to be more stable when it runs with the collimator installed on the rotating plate and the aluminum panels on its sides. The configuration with the lead bricks on top of the chopper improved the performances of the old design. However, with the new design, their weight introduces a small instabilities above 10 Hz which are not present with the configuration without the lead bricks.